Nanoscale

Accepted Manuscript

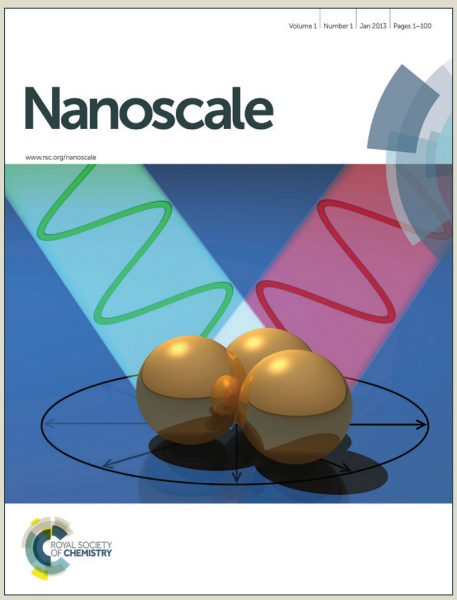

ROYAL SOCIETY OF CHEMISTRY

www.rsc.org/nanoscale

Journal Name

RSCPublishing

ARTICLE

Fabrication of mesoporous metal oxide coated-nano carbon hybrid materials via a polyol-mediated self-assembly process

Bingmei Feng,[1] Huixin Wang,[1] Dongniu Wang,[1] Huilong Yu,[2] Yi Chu,[1] Hai-Tao FANG[1]*

[1]School of Materials Science and Engineering, Harbin Institute of Technology, Harbin 150001, P. R. China

[2]National Key Laboratory for Surface Physics and Chemistry, Mianyang 621907, P. R. China

Corresponding author: htfang@hit.edu.cn

After clarifying the formation mechanism of a typical metal glycolate precipitate, Ti glycolate, in a polyol-mediated synthesis using acetone as a precipitation media, we describe a simple template-free approach based on an ethylene glycol-mediated synthesis to fabricate mesoporous metal oxide coated-nano carbon hybrid materials including TiO_2 coated-carbon nanotube (CNT), SnO_2 coated-CNT, Cu_2O/CuO coated-CNT and TiO_2 coated-graphene sheet (GS). In the approach, metal oxide precursors, metal glycolates, were first deposited on CNTs or GSs, subsequently transformed to the metal oxide coatings by a pyrolysis or hydrolysis. By a comparison between the characterizations of two TiO_2-CNT hybrid materials used carboxylated CNTs and pristine CNTs without carboxyl groups, the driving force for initiating the deposition of metal glycolates on the carboxylated CNTs is confirmed to be the hydrogen bonding between the carboxyl groups and the polymer chains in metal glycolate sols. The electrochemical performances of the mesoporous TiO_2 coated-carboxylated CNT and TiO_2-prinstine CNT hybrid materials were investigated. The results show that the mesoporous TiO_2 coated-carboxylated CNT with uniform core-shell nanostructure exhibits substantial improvement in rate performance in comparison with its counterpart from 0.5 C to 100 C because of its higher electronic conductivity and shorter diffusion path for lithium ion. At

the extremely high rate of 100 C, the specific capacity of TiO_2 of the former reaches 85 mAh/g, twice as high as that of the latter.

1 Introduction

Mesoporous metal oxides have attracted much attention in the application of photocatalysis,[1] electrocatalysis,[2] lithium ion batteries,[3] supercapacitors,[4] sensors,[5] and so on, as the rich mesopores and high surface areas favor the improvement of their performance. However, most metal oxides suffer from their low electrical conductivity especially for applications involving electrochemical processes dependent on electron transfer, such as the lithium ion batteries, supercapacitors, fuel cells and dye sensitized solar cells. Presently, intensive efforts are devoted to resolve this problem by the incorporation with electronically conductive additives such as carbon materials,[6-10] metals,[11] RuO_2 [12] and conducting polymers.[13]

Nanocarbons such as amorphous carbon coating layers,[8,14-17] carbon nanotubes (CNTs)[9,18-26]and graphene sheets (GSs)[10,27-33] are most widely incorporated with metal oxides to improve the electrical conductivity. Amorphous carbon coating layers are usually realized through the carbonation of organic polymers, such as glucose,[14] soluble phenolic resin,[15] polyvinyl alcohol[16] and block copolymer,[17] at high temperatures under a reducing or inert atmosphere. The carbon layer is generally dispersed as amorphous form without best electrical conductivity due to the abundance of sp^3-bonded carbon. Even thick carbon coating layer results in the obstruction of ion diffusion.[8] In addition, the mesopores of metal oxides may be sacrificed during the coating process. In comparison, CNTs and GSs with abundant sp^2-bonded carbon atoms are more attractive due to their unique nanostructure, high electrical conductivity and tunability on surface chemistry. Up to now, several methods have been proposed to prepare mesoporous metal oxide coated-CNT or coated-GS hybrid materials, such as sol-gel processes,[18,28,29] hydrothermal synthesis,[10,19,20,26,30] and electrochemical deposition.[21] The deposition can be attained through the hydrogen bonding interaction,[22] covalent bonding interaction,[20] electrostatic self-assembly,[23,25,27,31] or π-π stacking

interaction.[24] During the preparation, the CNTs or GSs content, surfactant concentration, the pH values and other conditions generally need to be carefully adjusted, otherwise the agglomeration of metal oxides is serious. A facile and general synthesis of mesoporous metal oxide coated-CNT or coated-GS hybrid materials with high uniformity and dispersity in nano scale remains a major challenge.

Recently, a simple process based on polyol-mediated synthesis (PMS) has been adopted to fabricate mesoporous metal oxides. Taking advantage of the coordination ability of ethylene glycol (EG) with transitional metal ions, EG is explored as a cross-linking reagent to react with metal salts to form metal glycolate.[34] Glycolates with sphere structure can be obtained if an unprecipitated reaction solution of EG with metal salts is added into an acetone bath.[35] Then the mesoporous metal oxides can be formed by the hydrolysis[36] or pyrolysis[34,35] of glycolates. The pores are formed by the removal of carbonaceous molecular chains and no surfactant is used. In other words, this process has template-free feature. Furthermore, it is worth noting that this process is suitable for the fabrication of various mesoporous 1-dimensional metal oxides, such as TiO_2,[34] SnO_2,[34] V_2O_5,[37] Co_3O_4[38] and so on. These mesoporous metal oxides obtained from glycolate precursors have been used in the fields of lithium ion batteries,[37] gas sensors,[38,39] and photodegradation.[40] Taking into account the simplicity and wide suitability of this EG polymerization for the preparation of mesoporous metal oxides, it is worthwhile to extend this process to develop a new synthesis method for fabricating a variety of mesoporous metal oxide coated-nanocarbon hybrid materials.

Here, the fabrication of mesoporous metal oxide coated-nano carbon hybrid materials via the acetone-assisted PMS is presented and corresponding mechanism for the deposition is analyzed. At first, the formation mechanism of metal glycolates in an acetone bath is analyzed by a typical example, the synthesis of Ti glycolate. Based on the clarification on a key point for the formation of metal glycolates in acetone, that is, hydrogen bonding of glycolate polymer chains with molecules (such as water or formic acid) owning higher polarity than EG molecules, an appropriate strategy is laid out to attain the fabrication of metal glycolate coated-CNT and coated-GS hybrid materials. A crucial point in the strategy is the use of CNTs

and GSs with carboxyl groups. The hydrogen bonding between the carboxyl groups and the polymer chains can initiate the deposition in a self-assembly manner. Finally, metal glycolate coated-CNT and coated-GS precursors were converted into mesoporous metal oxide coated-CNT and coated-GS hybrid materials by the pyrolysis or hydrolysis. Moreover, electrochemical lithium ion insertion/extraction of a mesoporous TiO_2 coated-CNT hybrid material is demonstrated to show how the uniform incorporation of CNTs in nano scale is able to improve the rate capability of mesoporous TiO_2 evidently.

2 Experimental Section

Synthesis of Titanium Glycolate: Typically, 2.4 ml titanium acetylacetonate was added into 50 ml ethylene glycol at room temperature. This mixed solution was then refluxed at 85 ^oC for 12 h to get a polymer solution. The obtained polymer solution was poured into 170 ml acetone bath contained 6 ml water, then stirred for 1 h. The precipitate was filtered, washed with ethanol and dried in air at 50 ^oC.

Mesoporous TiO_2 Coated-Carboxylated CNT Hybrid: A process similar with the synthesis of Ti glycolate was applied to prepare Ti glycolate coated-carboxylated CNT (denoted as TiGly-cCNT) precursor. At first, 6 mL water and 0.2 g carboxylated CNTs (denoted as cCNTs, purchased from Shenzhen Nanotech Port Co., Ltd) were added into 170 mL acetone and dispersed with the aid of ultrasonication for 1 h. Then the polymer solution was added to prepare TiGly-cCNT precursor. The mesoporous TiO_2 coated-carboxylated CNT hybrid (denoted as mTiO_2-cCNT) was obtained by a hydrolytic decomposition. The detail process is as follows: 0.1 g TiGly-cCNT precursor was dispersed in 100 ml water and filtered through polycarbonate filter membrane (47 mm in diameter, 0.2 um pore size) to form a membrane, then the membrane was immersed in 25 ml water and hydrolyzed at boiling point for 1h, finally the product was washed with water and dried in air at 50 ^oC.

Mesoporous TiO_2 Coated-Carboxylated GS Hybrid: The preparation process of the Ti glycolate coated-carboxylated GS (denoted as TiGly-cGS) precursor is similar with the TiGly-cCNT precursor. The content of carboxyl GSs (denoted as cGSs, purchase from Nanjing XFNANO Materials Tech Co., Ltd) in

acetone bath was 0.1 g and the ultrasonic time was 6 h. The followed hydrolytic process is the same with that of the $mTiO_2$-cCNT hybrid.

Characterization: SEM and TEM observations were performed using a FEI Quanta 200F scanning electron microscopy and a FEI G^2 F30 transmission electron microscope, respectively. XRD was carried out on a Bruker D8 Discover X-ray powder diffractometer with monochromatized Cu Kα radiation (40 kV/40 mA). XPS spectra were measured by a Thermo Scientific K-Alpha X-ray photon-electron spectroscopy with Al Kα radiation (1486.6 eV). FT-IR spectra were measured by a Perkin Elmer Spectrum-One system from 4000 to 400 cm^{-1} at room temperature. The nitrogen adsorption and desorption isotherms were obtained with a Belsorp-mini II instrument at 77 K, all samples were degassed at 150 ^oC for 4 h under vacuum before measurements. TG-DSC analysis was performed using a NETZSCH STA 449C simultaneous thermal analyzer at heating rate of 10 K/min under air atmosphere.

Electrochemical Measurements: The study on electrochemical performance of the $mTiO_2$-CNT was conducted using 2032 coin-type cells, and evaluated by galvanostatic techniques at different current densities (The current density of 1C is 335 mAh/g based on the mass of TiO_2). For preparing working electrode, a mixture of the $mTiO_2$-CNT , carbon black, and poly (vinyl difluoride) at a weight ratio of 8:1:1, was pasted onto a copper foil, then pressed at 60 MPa and dried under vacuum at 120 ^oC for 10 h. The cells were assembled in an argon-filled glove box (Mbraun LABStar). A lithium metal foil and GF/D (whatman) porous film were used as a counter electrode and separator, respectively. The electrolyte consists of a solution of 1 M $LiPF_6$ in ethylene carbonate (EC)/dimethyl carbonate (DMC) (1:1 in volume).

3 Results and Discussion

3.1 Formation Mechanism of Metal Glycolates

In this section, the fabrication of a typical metal glycolate, Ti glycolate, is studied in detail to clarify the formation mechanism of metal glycolates. After the reaction of titanium acetylacetonate with EG at 85 ^oC for 12 h, a polymer sol in unreacted residual EG solvent is formed. The tyndall phenomenon of the sol is

shown in Scheme 1(a). This sol is stable in air at room temperature for several months without any precipitation. Referring to the structure of metal glycolates reported in papers,[34,41] the structure of the polymer is considered to be a chain-like complex with hydroxyl groups as shown in Scheme 1(a). Each polymer chain in EG solvent can interact with EG molecules by hydrogen bonding. A plenty of EG molecules surrounding each polymer chain prevent the precipitation of the polymer sol at room temperature.

The dielectric constant (ε) of acetone is 20.7, lower than 37.7 of EG. The lower dielectric constant, the lower polarity, means weaker hydrogen bonding strength between the polymer chains and solvent molecules. Therefore, after pouring the sol solution into an acetone bath, the interaction between EG molecules and polymer chains can be disturbed and weakened by acetone molecules. It becomes easier for the polymer chains to overcome hydrogen bonding with EG molecules by their energy of thermal motion, and the precipitation is prone to happen. In this situation, if a small amount of molecules with higher polarity (higher ε), such as water molecules (ε=80.4) and formic acid (ε=58.5), exist in the acetone bath, the polymer chains start to interact each other by stronger hydrogen bonding with the molecules in bridging connection style as shown in Scheme 1(a), then the precipitation happens. To summarize, there are three crucial factors for the precipitation. The first is a solvent environment with weaker polarity than EG solvent. The second is the presence of a few molecules with higher polarity than EG molecules. The third is stronger hydrogen bonding between the polymer chains and the molecules with higher polarity than EG molecules in the acetone bath.

If the hydrogen bonding between the polymer chains and a few molecules with higher polarity than EG molecules plays a key role in the precipitation of metal glycolates as indicated in Scheme 1(a), the precipitation rate should be dependent on the strength of the hydrogen bonding. The higher the hydrogen bonding strength is, the faster the precipitation is. To certify the precipitation mechanism shown in Scheme 1(a), therefore, the effect of molecule polarity of reagents mixed in the acetone bath on the precipitation rate was studied. As illustrated in Table S1, with the same content of water and formic acid in acetone bath,

the nucleation rate in acetone/water mixed solution is much faster than that in acetone/formic acid mixed solution, and the product quantity of the former is seven times more than the latter. The results shown in Table S1 are consistent with expected, thus proving the reasonability of the mechanism shown in Scheme 1(a).

Furthermore, the effect of water content in the acetone bath on the Ti glycolate precipitation is studied. The results are shown in Table S2. With increase of water content, the onset time and quantity of the Ti glycolate precipitate show an initial increase then followed by a decrease, and no product is obtained when pouring the polymer sol into pure water. The increase of the product quantity is due to that more water provides more hydrogen bonding to connect the polymer chains. But with further increase of water content, the solvent environment with weaker polarity than EG solvent is destroyed. In this case, abundant water does not initiate the precipitation, but act as a stabilizer like the EG of the stable polymer sol instead. The results of Table S2 also support the mechanism shown in Scheme 1(a). Figure S1 shows the SEM images of the samples listed in Table S1 and Table S2.

3.2 Fabrication of Mesoporous Metal Oxide Coated-CNT and Coated-GS Hybrid Materials

The previous section demonstrates that hydrogen bonding between water or formic acid molecules and the polymer chains is a driving force for the precipitation. If functional groups with higher polarity than EG molecules, such as carboxyl groups, are abundant on the surface of CNTs or GSs, hydrogen bonding between carboxyl groups and the polymer chains is able to initiate the deposition of metal glycolates on CNTs or GSs in a self-assembly manner. Therefore, carboxyl group functionalized CNTs and GSs were used to prepare metal glycolate coated-CNT and coated-GS hybrid materials. The mechanism for the deposition on CNTs is shown in Scheme 1(b).

The metal glycolates can be decomposed into mesoporous metal oxides by the pyrolysis or hydrolysis.[34-36] Accordingly, mesoporous metal oxide coated-CNT and coated-GS hybrid materials can be obtained by the pyrolytic or hydrolytic decomposition of their precursors, metal glycolate coated-CNT and coated-GS

precursors, respectively. In this section, the fabrication and characterization of mesoporous TiO_2 coated-carboxylated CNT ($mTiO_2$-cCNT), SnO_2 coated-carboxylated CNT ($mSnO_2$-cCNT), Cu_2O/CuO coated-carboxylated CNT (mCu_2O/CuO-cCNT) and TiO_2 coated-carboxylated GS ($mTiO_2$-cGS) hybrid materials are described.

An SEM image of TiGly-cCNT precursor is presented in Figure 1a, in which only 1-dimensional structures are observed. The TiGly-cCNT precursor is converted into anatase TiO_2-cCNT after hydrolytic decomposition in boiling water. This conversion is confirmed by the XRD spectrum of the product after the hydrolytic decomposition (see Figure S2). The 1-dimensional morphology was preserved after the decomposition as indicated in SEM observation (Figure 1b) and TEM observation in low magnification (Figure 1c). The TiO_2 coating layer is 19-25nm thick, and many nanopores among the particles exist in the TiO_2 coating is clearly shown in Figure 1d. Figure 1e shows that the TiO_2 particles are highly crystalline. The N_2 adsorption-desorption measurement was conducted to investigate the pore structure. As shown in Figure 1f, the $mTiO_2$-cCNT exhibits the type IV isotherms with a distinct hysteresis loop at the relative pressure P/P_0 ranging from 0.4 to 0.9. This loop is a characteristic of mesopores. A comparison on the BJH pore size distribution of the $mTiO_2$-cCNT and bare cCNTs, presented in the inset of Figure 1f, demonstrates that the nanopores in the hybrid distribute more in 2-12 nm but much less in >12 nm. The increase of pore size distribution in 2-12 nm is attributed to the mesoporous nature of the TiO_2 coating. Nanopores of cCNTs larger than 15 nm are sacrificed due to the uniform shell of TiO_2 nanoparticles. The specific area of the $mTiO_2$-cCNT is as high as 198.5 m^2/g.

In order to clarify the function of the carboxyl groups for deposition, a pristine CNTs (denoted as pCNTs) sample without carboxyl groups was used to prepare a mesoporous TiO_2-pristine CNT hybrid material (denoted as $mTiO_2$-pCNT) under the same conditions for the preparation of the $mTiO_2$-cCNT. Figure 2 shows the C_{1S} X-ray photoelectron spectroscopy (XPS) analysis of pCNTs and cCNTs. The C_{1S} spectrum can be fitted with four peaks at 283.9, 284.8, 285.7, and 288.1 eV. The peaks at 283.9 eV and 284.8 eV are

attributed to sp^2 carbon and sp^3 carbon, respectively. The peak at 285.7eV is from the hydroxyl carbon (C-O), and the peak at 288.1eV is from the O=C-O functional group. Clearly, no C=O group is detected in the pCNTs.

The SEM image of Ti glycolate-pristine CNT (denoted as TiGly-pCNT) precursor in Figure 3a shows that lots of Ti glycolate sphere agglomerates exist in this hybrid. Further TEM observations of the $mTiO_2$-pCNT in Figure 3b, c show that only a few discontinuous TiO_2 particles are deposited and the most region of the pCNTs are uncovered. Obviously, upon the lack of strongly polar groups, such as carboxyl groups, on the CNTs, the polymer chains of Ti glycolate tends to spontaneously agglomerate and grow as sphere in acetone solution. Both of the pCNTs and cCNTs have hydroxyl groups as shown in Figure 2. But the hydroxyl groups can not initiate the deposition due to their lower polarity than EG molecules. For reference, the dielectric constant of methanol is 32.7 lower than that of EG. The comparison between the $mTiO_2$-pCNT and $mTiO_2$-cCNT further confirm the importance of the carboxyl groups for uniform coating. It is interesting to note the difference on the temperature of exothermic peak due to oxidation of CNTs for the two precursors. Figure S3a shows that the peak temperature for the TiGly-pCNT precursor is 625 ^oC, only 6 ^oC ahead in comparison with that of the pCNTs. The peak temperature for TiGly-cCNT precursor is 570 ^oC, 58 ^oC lower than the cCNTs, as shown in Figure S3b. As the reduction on the temperature of the maximum weight loss rate of CNT oxidation could be used to evaluate the uniformity of oxidation-catalyst metal oxide-CNT hybrid materials in macroscopic quantity,[42] the much higher shift of exothermic peak for the $mTiO_2$-cCNT reflects its much better uniformity in nano scale. In order to confirm the universality of the acetone-assisted PMS for preparation of mesoporous metal oxide coated-nano carbon hybrid materials, we attempted to fabricate $mSnO_2$-cCNT and mCu_2O/CuO-cCNT materials by the same fabrication route for the $mTiO_2$-cCNT. The details are included in Supporting Information (see Figure S4, S5 and related description).

The acetone-assisted PMS is not only suitable to fabricate metal oxide coated-CNT hybrid materials, but also adaptable to the fabrication of hybrid materials incorporated with other nanocarbons, such as GSs. Following, an example, the fabrication of $mTiO_2$-cGS is described. The cGSs have abundant carboxyl groups as shown in Figure 4a. From SEM images in Figure 4b, c, the TiGly-cGS precursor has the same morphology as the cGSs indicating a uniform coating of Ti glycolate. The elemental mapping analysis and TG-DSC curves in Figure S6 further prove that the Ti glycolate is uniformly distributed on cGSs. Figure 4d displays the FT-IR spectra of the cGSs before and after coating. The cGSs shows an obvious absorption peak of C=O stretching vibration at 1739 cm^{-1}. This adsorption peak does not move to lower wavenumber after coating, confirming the interaction between the hydroxyl groups of the Ti glycolate and the carboxyl groups of the cGSs is hydrogen bonding but not esterification reaction.[43] This conclusion also works for TiGly-cCNT. XRD spectra in Figure S6c confirm the conversion of the TiGly-cGS precursor into the $mTiO_2$-cGS after a hydrolytic decomposition. From the SEM images of the $mTiO_2$-cGS in Figure 4e, f, the morphology of the precursor was also reserved after the hydrolytic decomposition except the surface roughness because of the generation of mepororous TiO_2. A TEM image (Figure 4g) shows the presence of abundant nanopores on a cGS in the TiO_2 coating. Lattice fringe of anatase TiO_2 and mesopores with diameter of about 3nm are clearly displayed in a HRTEM image (Figure 4h). A N_2 adsorption analysis (Figure 4i) indicates that the mesopores of the $mTiO_2$-cGS distributed mainly between 2-10 nm are from the TiO_2 coating, the specific area of the $mTiO_2$-cGS is 172.0 m^2/g.

Furthermore, based on the sol-gel characteristics of the acetone-assisted PMS, it is easy to apply this process to attain various cationic dopings for transition metal oxides only through mixing different glycolate-polymer sol solutions in a suitable content. For instance, using mixture of Ti glycolate-polymer sol with Zr glycolate-polymer sol, a hybird of CNT with an uniform coating of nanoporous Zr-doped TiO_2 was obtained by our group.[44] Recently, a similar strategy involved a EG polyol process and subsequent thermal annealing treatment was adopted by Lou to prepare CNF@MnO and CNF@$CoMn_2O_4$ coaxial

nanocables.[45] Heating EG solutions but not the acetone-assisted PMS at room temperature was used by Lou to precipitate glycolate precursors. Comparing two strategies, the acetone-assisted PMS has advantage of avoiding possible separate precipitation of glycolates at high temperatures.

3.3 Electrochemical Performance of Mesoporous TiO_2 Coated-CNT Hybrid

The performance for electrochemical lithium ion insertion/extraction of the $mTiO_2$-cCNT and $mTiO_2$-pCNT was compared. Figure 5a shows their first charge-discharge curves at 0.5 C. Each discharge process can be divided into three stages. The first stage shows a fast voltage drop to about 1.7 V. The second stage is the voltage plateau region of lithium ion insertion into the lattice of TiO_2. The third stage is a gradual potential decay of surface insertion of lithium ion.[46] Apparently the two samples deliver a specific capacity based on the mass of TiO_2 slightly higher than the theoretical value of 335 mAh/g. This is probably because of the trapping of inserted lithium ions in the tiny micropores and surface -OH groups of TiO_2, as well as defects in CNTs. It should be pointed out that the $mTiO_2$-cCNT is able to deliver higher discharge and charge capacities in comparison with the $mTiO_2$-pCNT. But the coulomb efficiency of the $mTiO_2$-cCNT at the first cycle is 63.4%, a little lower than 67.7% of the $mTiO_2$-pCNT, probably due to more defects in carboxylated CNTs. As the discharge/charge rate increases from 0.5 to 100C (Figure 5b), the specific capacity of the $mTiO_2$-pCNT drops quickly than the $mTiO_2$-cCNT especially at higher rates. At the extremely rate of 100C, the specific capacity of $mTiO_2$-cCNT is 85 mAh/g, twice as high as specific capacity (40 mAh/g) of the $mTiO_2$-pCNT. The uniform core-shell nanostructure of the $mTiO_2$-cCNT offers not only higher electronic conductivity but also shorter diffusion path for lithium ion of liquid electrolyte in the mesopores of TiO_2 component in comparison with the $mTiO_2$-pCNT. After rate test, two electrodes were cycled at 1 C for long time (Figure 5c). Initially, the capacity can be resumed, 208 mAh/g and 196 mAh/g for $mTiO_2$-cCNT and $mTiO_2$-pCNT, respectively, suggesting the good structural stability of the sample at high charge-discharge rates. After 600 cycles of charge and discharge, 87% and 90% capacities can be reserved for $mTiO_2$-cCNT and $mTiO_2$-pCNT respectively.

4 Conclusion

The study on the formation mechanism of the Ti glycolate demonstrates that the hydrogen bonding between the polymer chains and a few added molecules with higher polarity than EG molecules plays a key role in the precipitation. A simple template-free approach based on an ethylene glycolate-mediated synthesis is developed to fabricate the mTiO_2-cCNT, mSnO_2-cCNT, mCu_2O/CuO-cCNT and the mTiO_2-cGS. These successful cases indicate the universality of the acetone-assisted PMS for fabricating other mesoporous metal oxide coated-nano carbon hybrid materials. By a comparison between the characterizations of mTiO_2-cCNT and mTiO_2-pCNT, the surface carboxyl groups of cCNTs or cGSs are crucial for the deposition of metal glycolates in a self-assembly manner. The driving force for the deposition is confirmed to be the hydrogen bonding between the carboxyl groups and the polymer chains of metal glycolate sols. Benefiting from the uniform core-shell nanostructure, the mTiO_2-cCNT exhibits better rate capability than mTiO_2-pCNT for electrochemical lithium ion insertion/extraction.

Acknowledgements

This work was supported by the National Natural Science Foundation of China (Grant nos. 51272051, 50872026 and 50602011), and the Research Fund for the Doctoral Program of Higher Education of China (20112302110014).

Notes and references

1 H. X. Li, Z. F. Bian, J. Zhu, D. Q. Zhang, G. S. Li, Y. N. Huo, H. Li, Y. F. Lu, J. Am. Chem. Soc., 2007, **129**, 8406-8407.

2 H. G. Lin, X. B. Ji, Q. Y. Chen, Y. K. Zhou, C. E. Banks, K. B. Wu, Electrochem Commun., 2009, **11**, 1990-1995.

3 K. Saravanan, K. Ananthanarayanan, P. Balaya, Energy Environ. Sci., 2010, **3**, 939-948.

4 Y. T. Wang, A. H. Lu, H. L. Zhang, W. C. Li, J. Phys. Chem. C., 2011, **115**, 5413-5421.

5 T. Waitz, T. Wagner, T. Sauerwald, C. D. Kohl, M. Tiemann, Adv. Funct. Mater., 2009, **19**, 653-661.

6 J. G. Yu, T. T. Ma, G. Liu, B. Cheng, Dalton T., 2011, **40**, 6635-6644.

7 G. R. Li, Z. P. Feng, Y. N. Ou, D. C. Wu, R. W. Fu, Y. X. Tong, Langmuir, 2010, **26**, 2209-2213.

8 S. K. Das, S. Darmakolla, A. J. Bhattacharyya, J. Mater. Chem., 2010, **20**, 1600-1606.

9 Z. H. Wen, Q. Wang, Q. Zhang, J. H. Li, Adv. Funct. Mater., 2007, **17**, 2772-2778.

10 J. Su, M. H. Cao, L. Ren, C. W. Hu, J. Phys. Chem. C., 2011, **115**, 14469-14477.

11 F. F. Cao, S. Xin, Y. G. Guo, L. J. Wan, J. Phys. Chem. Chem. Phys., 2011, **13**, 2014-2020.

12 Y. G. Guo, Y. S. Hu, W. Sigle, J. Maier, Adv. Mater., 2007, **19**, 2087-2091.

13 C. Lai, G. R. Li, Y. Y. Dou, X. P. Gao, Electrochim. Acta, 2010, **55**, 4567-4572.

14 Y. Chen, Q. Z. Huang, J. Wang, Q. Wang, J. M. Xue, J. Mater. Chem., 2011, **21**, 17448-17453.

15 R. L. Liu, Y. J. Ren, Y. F. Shi, F. Zhang, L. J. Zhang, B. Tu, D. Y. Zhao, Chem. Mater., 2008, **20**, 1140-1146.

16 M. Inagaki, Y. Hirose, T. Matsunaga, T. Tsumura, M. Toyoda, Carbon, 2003, **41**, 2619-2624.

17 Z. C. Yang, J. G. Shen, L. A. Archer, J. Mater. Chem., 2011, **21**, 11092-11097.

18 I. Moriguchi, R. Hidaka, H. Yamada, T. Kudo, H. Murakami, N. A. Nakashima, Adv. Mater., 2006, **18**, 69-73.

19 C. Y. Du, M. Chen, X. Y. Cao, G. P. Yin, P. F. Shi, Electrochem. Commun., 2009, **11**, 496-498.

20 J. G. Yu, T. T. Ma, S. W. Liu, Phys. Chem. Chem. Phys., 2011, **13**, 3491-3501.

21 H. Zhang, G. P. Cao, Z. Y. Wang, Y. S. Yang, Z. J. Shi, Z. N. Gu, Nano Lett., 2008, **8**, 2664-2668.

22 Y. He, L. Huang, J. S. Cai, X. M. Zheng, S. G. Sun, Electrochim. Acta, 2010, **55**, 1140-1144.

23 Z. H. Wen, Q. Wang, Q. Zhang, J. H. Li, Adv. Funct. Mater., 2007, **17**, 2772-2778.

24 D. Eder, A. H. Windle, Adv. Mater., 2008, **20**, 1787-1793.

25 H. W. Huang, Y. Liu, J. H. Wang, M. X. Gao, X. S. Peng, Z. Z. Ye, Nanoscale., 2013, **5**, 1785-1788.

26 L. Zhang, G. Q. Zhang, H. B. Wu, L. Yu, X. W. Lou, Adv. Mater., 2013, **25**, 2589-2593.

27 D. Y. Chen, G. Ji, Y. Ma, J. Y. Lee, J. M. Lu, ACS Appl. Mater. Interfaces, 2011, **3**, 3078-3083.

28 Z. S. Wu, D. W. Wang, W. Ren, J. Zhao, G. M. Zhou, F. Li, H. M. Cheng, Adv. Funct. Mater., 2010, **20**, 3595-3602.

29 H. Q. Cao, B. J. Li, J. X. Zhang, F. Lian, X. H. Kong, M. Z. Qu, J. Mater. Chem., 2012, **22**, 9759-9766.

30 J. Lu, M. Y. Wang, Y. Li, C. H. Deng, Nanoscale, 2012, **4**, 1577-1580.

31 C. Chen, L. J. Wang, Y. Y. Liu, Z. W. Chen, D. Y. Pan, Z. Li, Z. Jiao, P. F. Hu, C. H. Shek, C. M. L. Wu, J. K. L. Lai, M. H. Wu, Langmuir, 2013, **29**, 4111-4118.

32 H. Seema, K. C. Kemp, V. Chandra, K. S. Kim, Nanotechnology, 2012, **23**, 355705-355713.

33 R. W. Mo, Z. Y. Lei, K. N. Sun, D. Rooney, Adv. Mater., 2014, **26**, 2084-2089.

34 X. C. Jiang, Y. L. Wang, T. Herricks, Y. N. Xia, J. Mater. Chem., 2004, **14**, 695-703.

35 X. C. Jiang, T. Herricks, Y. N. Xia, Adv. Mater., 2003, **15**, 1205-1209.

36 L. S. Zhong, J. S. Hu, L. J. Wan, W. G Song, Chem. Commun., 2008, **10**, 1184-1186.

37 A. M. Cao, J. S. Hu, H. P. Liang, L. J. Wan, Angew. Chem. Int. Edit., 2005, **44**, 4391-4395.

38 A. M. Cao, J. S. Hu, H. P. Liang, W. G. Song, L. J. Wan, X. L. He, X. G. Gao, S. H. Xia, J. Phys. Chem. B, 2006, **110**, 15858-15863.

39 Y. L. Wang, X. C. Jiang, Y. N. Xia, J. Am. Chem. Soc., 2003, **125**, 16176-16177.

40 S. Z. Kang, Z. Z. Xu, Y. X. Song, J. J. Mu, Disperson Sci. Technol., 2006, **27**, 857-859.

41 D. Wang, R. B. Yu, N. Kumada, N. Kinomura, Chem. Mater., 1999, **11**, 2008-2012.

42 H. T. Fang, M. Liu, D. W. Wang, X. H. Ren, X. Sun, Nano Energy, 2013, **2**, 1232-1242.

43 F. A. Abuilaiwi, T. Laoui, M. Al-Harthi, M. A. Arab. Atieh, J. Sci. Eng., 2010, **35**, 37-48.

44 H. T. Fang, B. M. Feng, H. X. Wang, D. N. Wang, H. L. Yu (Harbin Institute of Technology), CN 201010109943, 2012.

45 G. Q. Zhang, H. B. Wu, H. E. Hoster, X. W. Lou, Energy Environ. Sci., 2014, **7**, 302-305.

46 Y. G. Guo, Y. S. Hu, J. Maier, Chem. Commun., 2006, **26**, 2783-2785.

Scheme 1. Formation mechanism of (a) the Ti glycolate and (b) the metal glycolate coated-CNT hybrid materials in acetone/water mixed solution.

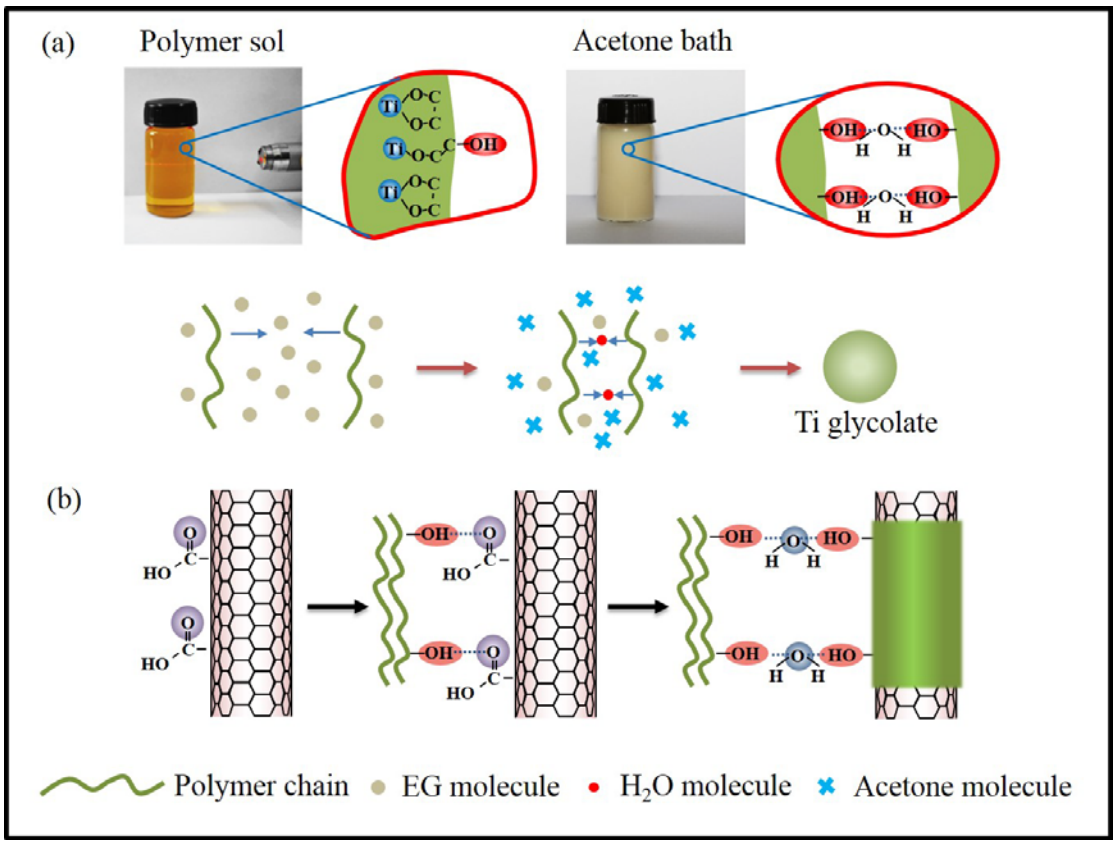

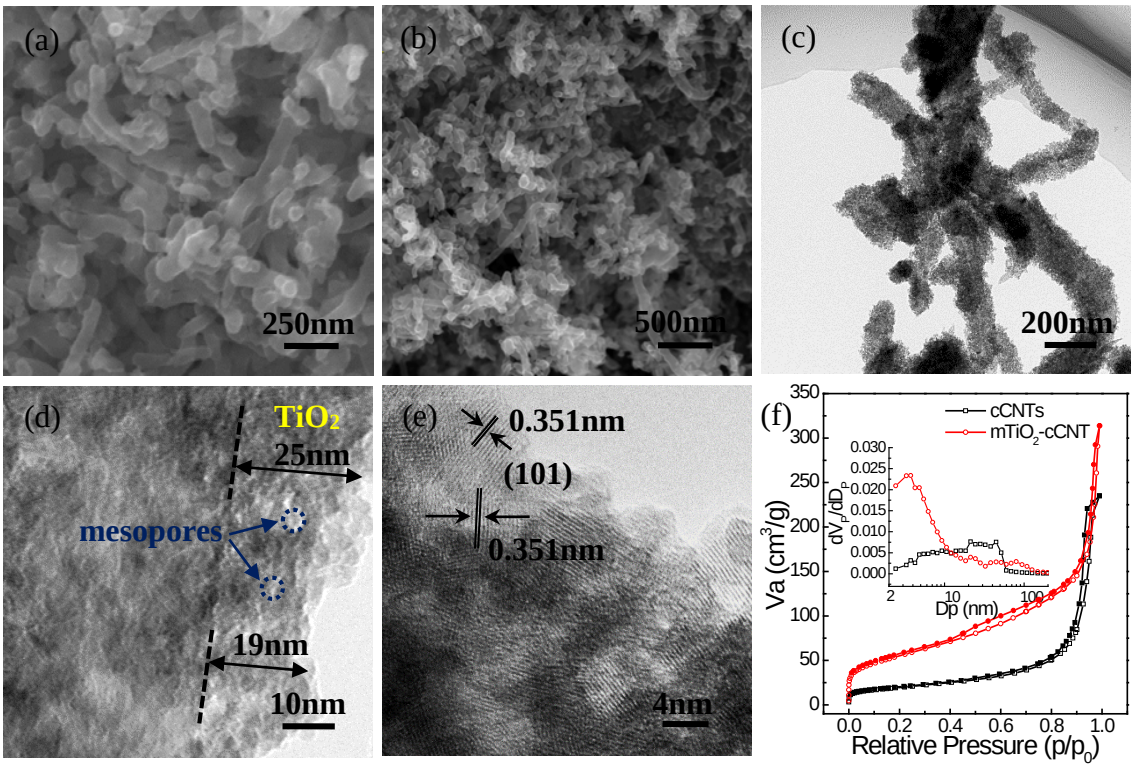

Figure 1. (a) SEM image of the TiGly-cCNT precursor. (b) SEM image, (c, d) TEM images and (e) HRTEM image of the $mTiO_2$-cCNT. (f) N_2 adsorption-desorption curves and BJH pore size distribution curves (insert) of the cCNTs and $mTiO_2$-cCNT.

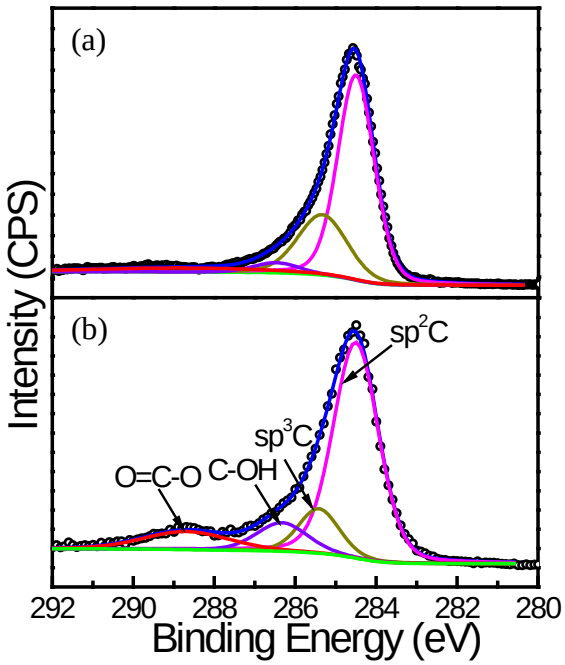

Figure 2. XPS spectra of (a) pristine CNTs and (b) carboxylated CNTs.

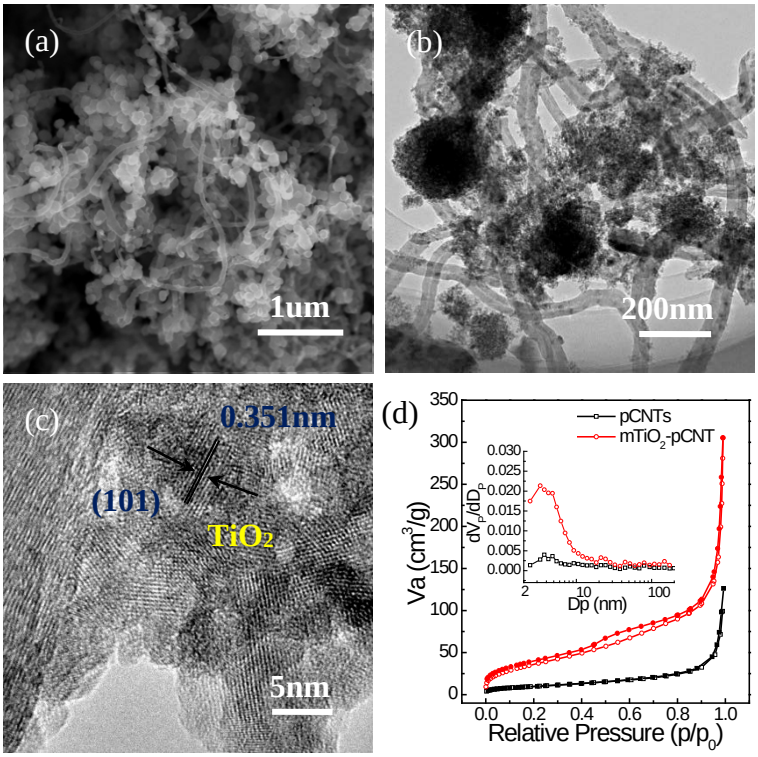

Figure 3. (a) SEM image of the TiGly-pCNT precursor. (b) TEM image and (c) HRTEM image of the $mTiO_2$-pCNT. (d) N_2 adsorption-desorption curves and BJH pore size distribution curves (insert) of the pCNTs and $mTiO_2$-pCNT.

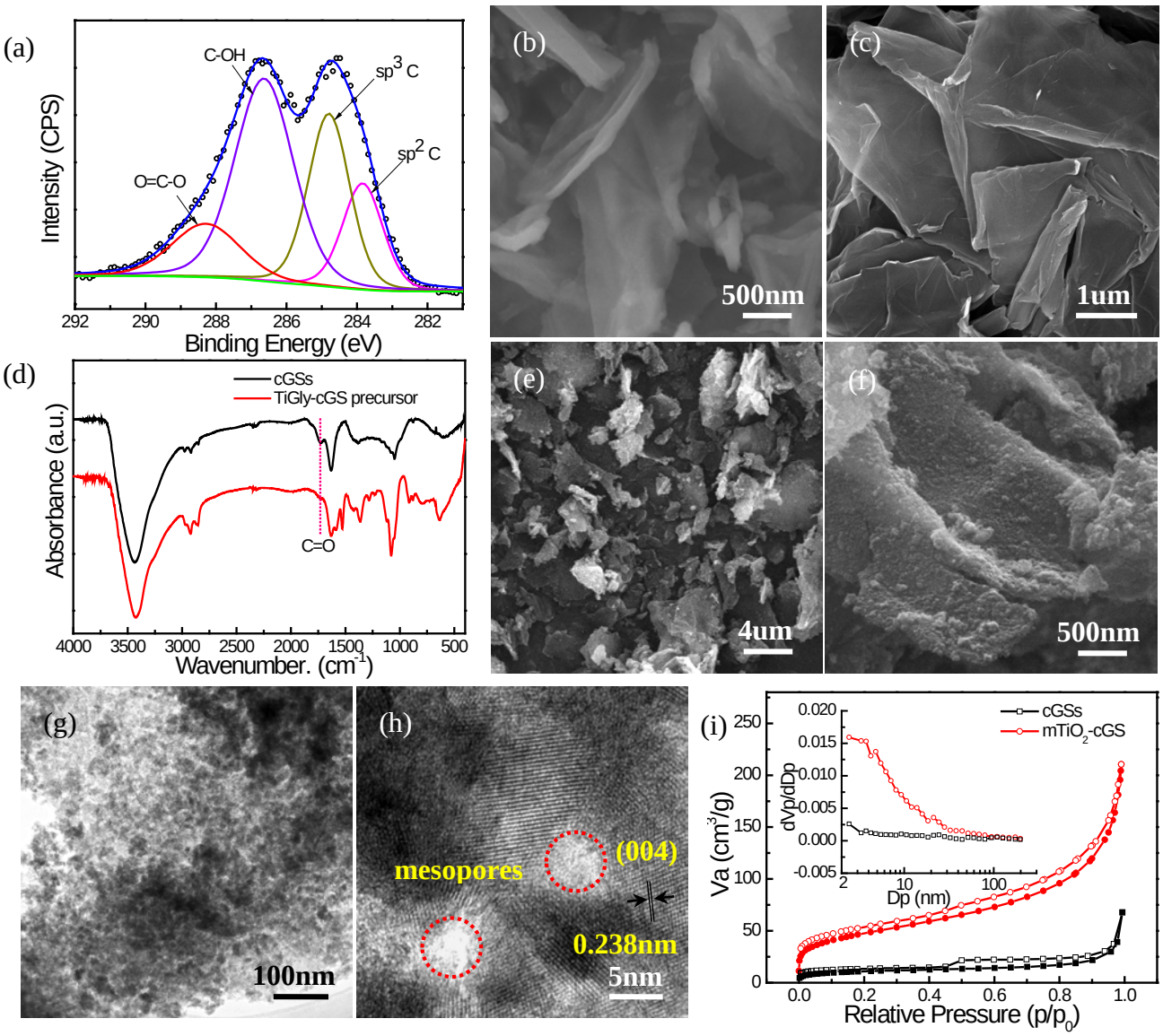

Figure 4. (a) XPS spectra of the cGSs. SEM images of (b) the cGSs and (c) the TiGly-cGS precursor. (d) FT-IR spectra of the cGSs and TiGly-cGS precursor. (e, f) SEM images, (g) TEM image and (h) HRTEM image of the $mTiO_2$-cGS. (i) N_2 adsorption-desorption curves and BJH pore size distribution curves (insert) of the cGSs and $mTiO_2$-cGS.

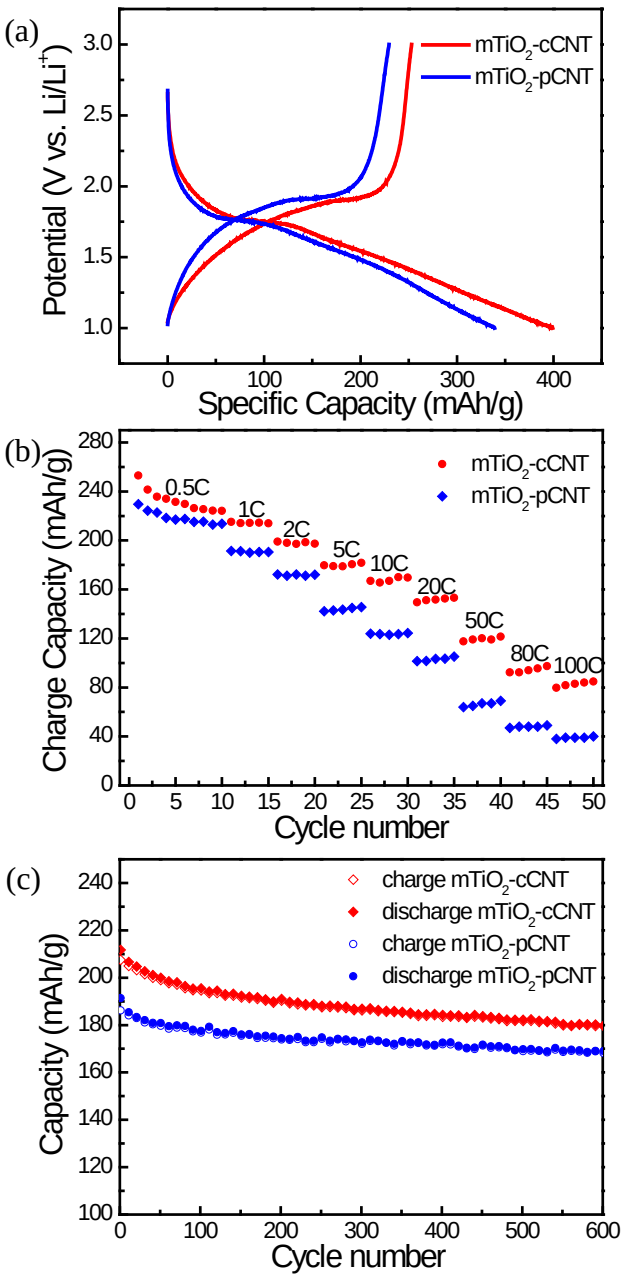

Figure 5. (a) First charge-discharge curves of the $mTiO_2$-cCNT and $mTiO_2$-pCNT at 0.5C. (b) Rate capability of the $mTiO_2$-cCNT and $mTiO_2$-pCNT. (c) Cycling performance of the $mTiO_2$-cCNT and $mTiO_2$-pCNT at 1C after measuring the rate capability.